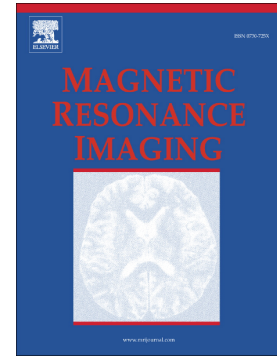


Accepted Manuscript

Improved coronary magnetic resonance angiography using gadobenate dimeglumine in pediatric congenital heart disease

Miguel Silva Vieira, Markus Henningsson, Nathalie Dedieu, Vassilios S. Vassiliou, Aaron Bell, Sujeev Mathur, Kuberan Pushparajah, Carlos Alberto Figueroa, Tarique Hussain, René Botnar, Gerald F. Greil



PII: S0730-725X(17)30309-0
DOI: <https://doi.org/10.1016/j.mri.2017.12.023>
Reference: MRI 8900

To appear in:

Received date: 27 August 2017
Revised date: 25 December 2017
Accepted date: 29 December 2017

Please cite this article as: Miguel Silva Vieira, Markus Henningsson, Nathalie Dedieu, Vassilios S. Vassiliou, Aaron Bell, Sujeev Mathur, Kuberan Pushparajah, Carlos Alberto Figueroa, Tarique Hussain, René Botnar, Gerald F. Greil , Improved coronary magnetic resonance angiography using gadobenate dimeglumine in pediatric congenital heart disease. The address for the corresponding author was captured as affiliation for all authors. Please check if appropriate. Mri(2017), <https://doi.org/10.1016/j.mri.2017.12.023>

This is a PDF file of an unedited manuscript that has been accepted for publication. As a service to our customers we are providing this early version of the manuscript. The manuscript will undergo copyediting, typesetting, and review of the resulting proof before it is published in its final form. Please note that during the production process errors may be discovered which could affect the content, and all legal disclaimers that apply to the journal pertain.

TITLE:**Improved coronary magnetic resonance angiography using gadobenate dimeglumine in pediatric congenital heart disease**

AUTHORS

Miguel Silva Vieira, MD, MPhil^{a*}

Email: miguel.silvavieira@kcl.ac.uk

Markus Henningsson^{a*}

Email: markus.henningsson@kcl.ac.uk

Nathalie Dedieu^b

Email: nathalie.dedieu@gosh.nhs.uk

Vassilios S Vassiliou^c

Email: v.vassiliou@rbht.nhs.uk

Aaron Bell, PhD^d

Email: aaron.bell@gstt.nhs.uk

Sujeev Mathur, MD^d

Email: sujeev.mathur@gstt.nhs.uk

Kuberan Pushparajah, MD^d

Email: kuberan.pushparajah@gstt.nhs.uk

Carlos Alberto Figueroa, PhD^{a,e}

Email: figueroc@med.umich.edu

Tarique Hussain, PhD^g

Email: mohammad.hussain@utsouthwestern.edu

René Botnar, PhD^{a,g}

Email: rene.botnar@kcl.ac.uk

Gerald F Greil, PhD^{a,g}

Email: gerald.greil@utsouthwestern.edu

^aDivision of Imaging Sciences & Biomedical Engineering, King's College London, London, UK

^bGreat Ormond Street Hospital for Children NHS Foundation Trust, London, UK

^cCMR Unit, Royal Brompton and Harefield NHS Foundation Trust, London, UK

^dEvelina Children's Hospital London, Guy's and St. Thomas' NHS Foundation Trust, London, UK

^eDepartments of Surgery and Biomedical Engineering, University of Michigan, Michigan, USA

^fPontificia Universidad Católica de Chile, Escuela de Ingeniería, Santiago, Chile

^gDepartment of Pediatrics, University of Texas Southwestern Medical Center, Dallas, USA

*contributed equally

Corresponding author: Dr Miguel Silva Vieira, Division of Imaging Sciences & Biomedical Engineering, King's College London, 4th Floor, Lambeth Wing St. Thomas' Hospital, London SE1 7EH, United Kingdom.

Email: miguel.silvavieira@kcl.ac.uk

Tel: +44 (0)20 718 88366; Fax: +44 (0)20 718 83056

ABSTRACT:

Background: CMRA in pediatrics remains challenging due to the smaller vessel size, high heart rates (HR), potential image degradation caused by limited patient cooperation and long acquisition times. High-relaxivity contrast agents have been shown to improve coronary imaging in adults, but limited data is available in children. We sought to investigate whether gadobenate dimeglumine (Gd-BOPTA) together with self-navigated inversion-prepared coronary magnetic resonance angiography (CMRA) sequence design improves coronary image quality in pediatric patients.

Methods: Forty consecutive patients (mean age 6 ± 2.8 years; 73% males) were prospectively recruited for a 1.5-T MRI study under general anesthesia. Two electrocardiographic-triggered free breathing steady-state free precession (SSFP) angiography sequences (A and B) with isotropic spatial resolution (1.3mm^3) were acquired using a recently developed image-based self-navigation technique. Sequence A was acquired prior to contrast administration using T2 magnetization preparation (T2prep). Sequence B was acquired 5-8 minutes after a bolus of Gd-BOPTA with the T2prep replaced by an inversion recovery (IR) pulse to null the signal from the myocardium. Scan time, signal-to noise and contrast-to-noise ratios (SNR and CNR), vessel wall sharpness (VWS) and qualitative visual score for each sequence were compared.

Results: Scan time was similar for both sequences (5.3 ± 1.8 vs 5.2 ± 1.5 minutes, $p=0.532$) and average heart rate (78 ± 14.7 vs 78 ± 14.5 bpm, $p=0.443$) remained constant throughout both acquisitions. Sequence B resulted in higher SNR (12.6 ± 4.4 vs 31.1 ± 7.4 , $p<0.001$) and CNR (9.0 ± 1.8 vs 13.5 ± 3.7 , $p<0.001$) and provided improved coronary visualization in all coronary territories (VWS A= 0.53 ± 0.07 vs B= 0.56 ± 0.07 , $p=0.001$; and visual scoring A= 3.8 ± 0.59 vs B= 4.1 ± 0.53 , $p<0.001$). The number of non-diagnostic coronary segments was lower for sequence B [A=42 (13.1%) segments vs B=33 (10.3%) segments; $p=0.002$], and contrary to

the pre-contrast sequence, never involved a proximal segment. These results were independent of the patients' age, body surface area and HR.

Conclusions: The use of Gd-BOPTA with a 3D IR SSFP CMRA sequence results in improved coronary visualization in small infants and young children with high HR within a clinically acceptable scan time.

Key words: Gadobenate dimeglumine; respiratory image-based navigation; coronary magnetic resonance angiography; pediatric congenital heart disease.

ACCEPTED MANUSCRIPT

Abbreviations list:

BP-CA – blood pool contrast agent	ECG – electrocardiogram
BSA – body surface area	Gd-BOPTA – gadobenate dimeglumine
SSFP – steady state free precession	HR – heart rate
CHD – congenital heart disease	iNAV – image-based navigator
CMR – cardiovascular magnetic resonance	IR – inversion recovery
CMRA – coronary magnetic resonance angiography	LAD – left anterior descending artery
CNR – contrast-to-noise ratio	LCx – left circumflex artery
CoA – aortic coarctation	MRI – magnetic resonance imaging
EC-GBCA – extra-cellular gadolinium-based contrast agent	RCA – right coronary artery
	SNR – signal-to-noise ratio
	VWS – vessel wall sharpness

INTRODUCTION

Three-dimensional (3D) whole-heart coronary magnetic resonance angiography (CMRA) is a well-established technique to assess cardiovascular morphology and coronary anatomy in patients with congenital heart disease (CHD) (1-3). The ability of CMRA to reliably identify the origin and proximal course of the coronary arteries and the desire to minimize radiation exposure makes this an ideal modality to image infants and young children with suspected coronary anomalies.

CMRA is typically acquired during free breathing using an electrocardiographic (ECG) triggered steady-state free-precession (SSFP) readout and T2-preparation pulses to generate contrast between blood and myocardium. It is frequently combined with a fat-suppression technique to eliminate the signal from epicardial and mediastinal fat (3).

Conventionally, a respiratory navigator positioned on the diaphragm has been used to suppress respiratory motion artifacts by only accepting data acquired in a predefined respiratory gating window (4). More recently, improved respiratory motion compensation has been achieved using 1D or image-based self-navigation, whereby motion is measured directly on the heart. This has been shown to out-perform the conventional respiratory motion compensation approach and to improve image quality (5-7).

Although in most adult cases the origin and proximal course of the coronary arteries can be visualized by non-contrast enhanced CMRA, coronary imaging in pediatrics remains challenging and the experience is still limited (1,2,8). In fact, despite ongoing advances in CMRA sequence development and post-processing techniques, a number of factors can result in lengthy and suboptimal imaging acquisitions: high heart rates (HR) therefore shorter rest periods (shorter diastasis, where cardiac motion is minimal and acquisition window is ideal for coronary imaging); irregular breathing (thus low respiratory tracking efficiency); small diameter of the coronary arteries; and poor contrast between the blood pool and extravascular

structures (e.g. pericardial fluid). Such acquisitions are prone to respiratory and cardiac motion artifacts. In recent years, respiratory image-based navigator (iNAV) techniques have been shown to improve image quality compared to conventional motion compensation, in patients with congenital heart disease. A further challenge of pediatric CMRA is that most images have relative lower spatial-resolution and signal-to-noise ratio (SNR) in comparison with their adult counterparts, thus reducing diagnostic accuracy. Finally, in many cases contrast-agents are given to assess myocardial perfusion and viability, which increases the SNR of SSFP sequences and thus improves image quality of CMRA (9-11).

Improved contrast may be achieved by replacing the T2 preparation pulses with an inversion-recovery (IR) pulse. This introduces heavy T1-weighting and thus is beneficial with the administration of a T1-shortening contrast-agent (12,13). In addition, signal from pericardial fluid (typically bright on T2-prepared CMRA) can be suppressed due to its long T1. In some subjects, high signal from fluid within the pericardial recesses with T2-prepared approaches can obscure the proximal coronary arteries.

Gd-BOPTA is a second-generation contrast agent. It has higher relaxivity compared to non-specific Gd-chelates due to binding to blood albumin, also called receptor induced magnetization enhancement (RIME) and consequently slower total blood clearance and longer plasma half-life, resulting in a higher and prolonged intravascular signal. The use of high-relaxivity contrast-agents has been shown to improve coronary imaging in adult patients, but limited data is available in pediatric patients (11,12,14,15).

The purpose of this study was to compare the use of a high-relaxivity contrast-agent, gadobenate dimeglumine (Gd-BOPTA, MultiHance; Bracco Imaging, Milan, Italy) in combination with specific sequence design to conventional T2-prepared 3D-SSFP CMRA in pediatric patients with CHD.

METHODS

Study population

The study was approved by the local institutional research ethics committee (South East London Research Ethic Committee, 10/H0802/65). Informed consent was obtained from all participants' parents/guardians prior to scanning. The inclusion criterion was children (age >2 years) with CHD with a clinically indicated cardiovascular magnetic resonance (CMR) study requiring general anesthesia referred to our Department. Exclusion criteria included any contra-indications to MRI (e.g. pacemakers), known allergy to MRI contrast-agents and impaired renal function.

Forty consecutive children over 2 years old were prospectively enrolled (September 2013 to February 2015). All scans were performed on a 1.5-T clinical scanner (Achieva, Philips Healthcare, Best, The Netherlands). All examinations were done under general anesthesia, following the local institutional practice for infants and small children and after careful weighting the benefits of a diagnostic examination, the developmental maturity and prior patient's experience, parents' insights of their child's capacity to cooperate with the study and the anticipated length of the CMR protocol.

Coronary MRA Sequence

The whole-heart CMRA scan consisted of an ECG-triggered 3D-SSFP sequence with the following imaging parameters: repetition time/echo time (TR/TE)=4.5/2.2ms; flip angle=70°; isotropic spatial resolution with an acquired voxel size of 1.3×1.3×1.3mm (0.65x0.65x0.65mm reconstructed voxel size); SENSE factor=2. Images were acquired using a 5-channel phased-array cardiac coil.

The CMRA acquisition had a coronal orientation with readout in foot–head direction, phase encoding in left–right direction and slice encoding in anterior–posterior direction. The coronal orientation was chosen to exclude the chest wall and minimize respiratory motion

artifacts. Data acquisition was synchronized with the ECG to coincide with the longest quiescent cardiac phase. The optimal trigger delay time and acquisition window were determined from an axial high-temporal resolution four-chamber cine. Single-phase studies were acquired and the longest rest period of the heart coinciding with the late-systolic or diastolic-phase images was determined primarily by evaluating the movement of the right coronary artery (RCA) (16).

The conventional pre-contrast coronary MRI sequence used a fat-suppression pre-pulse and T2-preparation pre-pulse to suppress signal from the myocardium and improve the blood-to-myocardium contrast (sequence A). Subsequently, contrast (Gd-BOPTA) was administered as a bolus by hand injection followed by 10 to 20 milliliters (mL) of a saline bolus (11). The post-contrast CMRA scan (sequence B) was performed approximately 5-8 minutes after the injection of Gd-BOPTA (0.2mL per kilogram of body-weight) following previous experience (9,17) and after a pre-study validation of the technique in five patients. This allowed the circulating contrast material to stabilize in the blood-pool and thereby avoid significant changes in the inversion-time during the post-contrast scanning. For the post-contrast CMRA scan, an IR-approach was used to null signal from the myocardium. The optimal inversion-time for nulling the myocardium was determined using a Look-Locker sequence prior to the post-contrast CMRA.

For respiratory motion compensation, both sequence A and B used a recently developed image-based navigator (iNAV) (18). In short, this method used the start-up echoes of the SSFP sequences to generate a low-resolution 2D projection image of the heart, with the same geometric properties as the whole-heart CMRA. The iNAV was then used to directly track and correct the respiratory motion of the heart in the foot-head and left-right directions. Additionally, respiratory gating with a constant efficiency of 50% was used to limit data acquisition to end-expiration.

The rest of the CMR protocol was dictated by the clinical indication and imaging findings, including conventional cine acquisitions in short and long-axis, phase-contrast flows and a time-resolved contrast-enhanced angiography with keyhole.

Data analysis

Quantitative analysis – Acquisition of a noise image required for global SNR and CNR calculations with parallel imaging was not considered practical due to time constraints (19). Nevertheless, by ensuring imaging parameters such as the patient position, field-of-view, matrix-size, flip-angle, phase-encoding direction and acceleration factor were unchanged between sequence A and B, and by selecting identical regions-of-interest (ROIs) in both sets of resulting images, a local SNR (SNR_l) and local CNR (CNR_l) were calculated as detailed:

$$SNR_l = \frac{I_B}{SD(L)}$$

$$CNR_l = \frac{I_B - I_M}{SD(L)}$$

where I_B and I_M refers to the mean signal-intensity in an ROI in the blood-pool (proximal ascending aorta) and myocardium (mid ventricular septum) respectively, and $SD(L)$ refers to the standard deviation of an ROI of air in the lungs (chosen to contain a minimum of 100 pixels while avoiding any visible vascular structures). These ROIs were specifically drawn in similar locations in both sequence A and B (MSV, 5 years of experience in CMR and Society of Cardiovascular Magnetic Resonance level 3 training) by using patient-specific landmarks.

Coronary reformatting and quantitative analysis of vessel length, diameter and wall sharpness was performed using a dedicated software ("Soap-Bubble", Philips Medical Systems, Best, The Netherlands), as previously described (12,20). This custom-made validated tool facilitates multiplanar reformats of CMRA datasets, while also providing

vessel length and diameter for objective quantitative comparison (figure 1 supplementary material). Furthermore, the local vessel wall sharpness (VWS) can be obtained by means of a Deriche algorithm (20,21), which is the basis of a semiautomated vessel-tracking tool to identify the vessel borders along the path. In brief, by using a first-order derivative (edge) of the input image, the local magnitude change in signal intensity can be calculated, which then provides a single VWS value for the entire path (a higher percentage magnitude change at the edge is consistent with superior sharpness).

Qualitative image analysis – Coronary image quality was determined on the basis of a 5-point grading system (table 1), which has been previously described (12). Analysis was performed by two independent experienced readers (reader 1 - ND, 4 years of experience in CMR; reader 2 - VV, 4 years of experience in CMR and Society of Cardiovascular Magnetic Resonance level 3 training). Grading involved careful visual inspection of the image quality of the proximal to distal segments of the coronary arteries of each patient dataset, according to the standardized American Heart Association (AHA) coronary segmentation model adapted for cardiovascular computed tomography angiography (22). Both readers were blinded to the study results or details of the sequences used to report the findings. Prior to the study analysis, agreement was assessed on illustrative coronary imaging cases not part of the study sample (figure 2 supplementary material).

Statistical Analysis

A sample size calculation was performed prior to the study to plan recruitment. Using a standard deviation of 10% taken from previous VWS measurements in congenital CMRA (23), a power level of 80%, and a significance level of 0.05 to detect a clinically significant change of 10% in vessel sharpness, 36 patients were estimated to be needed for bivariate analysis. Quantitative variables are expressed as mean \pm standard deviation (SD). Image quality and vessel length, diameter, and wall sharpness pre and post-contrast were compared

using the paired t test for parametric variables and with the Wilcoxon signed rank test for nonparametric variables. One-way ANOVA and Tukey HSD post hoc test were used to test for any difference in mean VWS values per coronary artery territory imaged with both pre and post-contrast sequences.

Intra- and inter-observer variability for the qualitative scores given to each coronary segments imaged with sequences A and B was evaluated using the 95% limits-of-agreement approach proposed by Bland and Altman (24) and the Cohen's kappa coefficient. This was performed for the 40 subjects enrolled and each independent reader was blinded to the details of the sequence used. For the intra-observer variability, each reader scored each coronary segment twice in different days to reduce any potential bias. For the inter-observer variability, the average qualitative score given to each coronary segment by one of the readers was compared to the results obtained by the other reader. The kappa coefficient of agreement was graded as follows: 0 to 0.2 = poor to slight; 0.21 to 0.4 = fair; 0.41 to 0.6 = moderate; 0.61 to 0.8 substantial; and 0.81 to 1.0 = nearly perfect (25).

Bivariate analyses were performed to assess any correlation between imaging parameters (VWS and qualitative score) and age, body surface area (BSA) and HR. Additionally, a multivariate linear regression model was built to explore if any of the patient's variables (age, BSA, and HR) predicted the coronary imaging results. Differences were considered statistically significant at a p value <0.05 (2-tailed). All statistical analyses were performed using SPSS version 22.0 (IBM SPSS Statistics, IBM Corporation, Armonk, New York).

RESULTS

Forty consecutive patients (mean age 6 ± 2.8 years; 73% males) were prospectively recruited. This constituted a very heterogeneous population in terms of clinical indications for the CMR study (table 2), that span from simple cardiac defects (e.g. atrial septal defects) to more complex CHD, representative of real-world referrals to a congenital CMR center. Figure 1 provides some examples of the coronary imaging results achieved with the two sequences. No adverse events or any contrast reaction were registered during this study.

Table 3 summarizes the coronary imaging parameters and attributes of the two sequences. Both sequence A (pre-contrast) and sequence B (post-contrast) had similar acquisition durations (A= 5.3 ± 1.8 vs B= 5.2 ± 1.5 minutes; $p=0.532$). Furthermore, there was no significant difference in the HR during both sequence acquisitions, with a mean HR of 78 ± 14.7 for sequence A vs 78 ± 14.5 bpm for sequence B ($p=0.443$). The average inversion time of sequence B was 234 ± 14.6 ms [210 – 260 ms]. The mean vessel length was 5.2 ± 1.8 (A) vs 6.4 ± 2.0 cm (B) ($p<0.001$) for a similar average vessel diameter of 2.2 ± 0.2 (A) vs 2.2 ± 0.2 mm (B) ($p=0.922$).

Five patients had coronary anomalies (table 4). Table 5 depicts the average qualitative score given by the two readers. There was substantial intra-observer (reader 1: sequence A $k=0.545$, $p<0.001$ and sequence B $k=0.782$, $p<0.001$; reader 2: sequence A $k=0.654$, $p<0.001$ and sequence B $k=0.743$, $p<0.001$) and inter-observer agreement (sequence A $k=0.75$, $p<0.001$; sequence B $k=0.717$, $p<0.001$) for the qualitative coronary scores given by the two independent readers (figures 3 and 4 supplementary material).

CMRA after Gd-BOPTA administration and acquired with a self-navigated IR SSFP sequence (B) resulted in significantly higher SNR (A= 12.6 ± 4.4 vs B= 31.1 ± 7.4 ; $p<0.001$) and CNR (A= 9.0 ± 1.8 vs B= 13.5 ± 3.7 ; $p<0.001$) compared to the pre-contrast self-navigated T2-prepared SSFP sequence (A).

Overall, higher coronary VWS ($A=0.53\pm 0.07$ vs $B=0.56\pm 0.07$; $p=0.001$) and qualitative scores ($A=3.8\pm 0.59$ vs $B=4.1\pm 0.53$; $p<0.001$) were achieved with sequence B as depicted in figures 2 and 3. Except for the left circumflex artery (LCx) VWS, this improvement was statistically significant in all coronary territories (table 5 and figure 3). The number of non-diagnostic coronary segments (score 1 and 2) was significantly lower for sequence B [$A=42$ (13.1%) vs $B=33$ (10.3%); $p=0.002$]. Furthermore, while there were three non-diagnostic proximal segments with sequence A (0.9%), all involving the LCx, there were none in the post-contrast sequence. In fact, it was in the LCx territory that both sequences had lower VWS and qualitative scores (table 5 and figure 3). However, when analyzing by coronary artery segment imaged, there were no statistically significant differences in the mean pre-contrast as well as in the mean post-contrast VWS as determined by one-way ANOVA (sequence A: $F(2, 117)=0.651$, $p=0.524$; sequence B: $F(2, 117)=1.83$, $p=0.164$).

In our study, the same trigger delay was used for both sequence A and B and ranged from 180 to 290 milliseconds (msec) for systolic-triggered scans and 430 to 759 msec for diastolic acquisitions. Two thirds of the acquisitions ($n=29$; 72.5%) were synchronized with the diastolic phase. On bivariate analysis, there was no correlation between the resting trigger delay selected and the coronary VWS for both sequence A ($R=0.071$, $p=0.663$) and B ($R=0.173$, $p=0.285$).

Finally, there was no correlation between patients' variables such as age, BSA or HR and coronary VWS results as summarized in figure 5 scatterplots. None of these patient's variables were shown to predict the coronary VWS values on the multiple linear regression analysis ($R^2=0.108$, $p=0.242$ for sequence A; $R^2=0.033$, $p=0.744$ for sequence B).

DISCUSSION

In this prospective crossover trial, a sample of infants and young children with CHD referred to our center were imaged using two self-navigated SSFP sequences (A and B). In both we used a novel self-navigation approach (a fixed respiratory gating efficiency 50% was applied) based on a recently developed 2D iNAV (26). In contrast to a 1D diaphragmatic navigation approach (1D NAV), the new iNAV sequence used allows direct estimation and correction of the respiratory induced bulk cardiac motion and diaphragm-heart hysteresis. This can improved CMRA image quality and does not require any dedicated planning for the navigator setup, nor any additional post-processing steps (18,26). More importantly, as gating efficiency for the iNAV sequence used was fixed at 50%, with the only the best 50% of the collected data used for image reconstruction, and all patients where scanned under general anesthesia (no change in the anesthetic procedure throughout the two experiments, with an average time interval between both of 18.05 ± 4.0 minutes), a head-to-head comparison of the two different CMRA acquisitions was possible.

Therefore, the only difference between the two sequences investigated was the magnetization preparation scheme. Sequence B used an IR pre-pulse instead of a T2prep and was acquired 5-8 minutes after administration of Gd-BOPTA.

Gd-BOPTA is a second-generation gadolinium contrast-agent, with a more lipophilic structure compared with conventional EC-GBCAs, which results in a weak and reversible interaction with serum albumin. This slows its extravasation out of the vascular space and increases its relaxivity compared to other agents, thus rendering a higher intravascular signal and improvement in diagnostic CMRA (11,15,27).

The T1 shortening effects and prolonged intravascular time of Gd-BOPTA, together with the changed magnetization preparation scheme resulted in the higher SNR seen in the retention equilibrium-phase images of the post-contrast sequence (table 3). In fact, sequence

B was specifically designed to benefit from the prolonged intravascular half-life of Gd-BOPTA and to increase the blood-to-background tissue contrast by means of an IR approach to null signal from the myocardium. This effect was also demonstrated by a significantly higher CNR. Because Gd-BOPTA resulted in a higher and stable intravascular signal, it also allowed isotropic high-spatial resolution imaging to be performed within a clinically feasible scan time of about five minutes, while also permitting dynamic vascular imaging with a single contrast injection (time-resolved angiography).

Adding the contrast to the novel sequence design resulted in a significant improvement in coronary visualization independent of age, BSA and HR, known to have detrimental effects on image quality. This improvement was also noted in all coronary territories and it was in fact independent of the vessel imaged or the resting cardiac phase chosen.

Notably, despite the fact that the mean vessel length obtained with sequence B was significantly higher than that of sequence A, both had similar mean vessel diameters. Although counterintuitive given the normal angiographic tapering of the coronary arteries, the post-contrast images had higher vascular signal and a better delineation of the wall, as demonstrated by a higher VWS. Because the vessel border was less clearly visualized before contrast injection, we hypothesize that signal loss due to partial volume artifact and noise resulted in underestimation of the true lumen in sequence A despite having the same spatial resolution as sequence B (28).

If on the one hand the prolonged intravascular half-life and high T1 relaxivity of Gd-BOPTA provides high homogenous signal that is not limited to the first-pass arterial-phase, on the other hand Gd-BOPTA can diffuse into the interstitial extracellular space due to its weak and reversible interaction with serum albumin and smaller molecules. However, this diffusion is slow, compared with EC-CAs (29), and so after setting the inversion time, the

myocardial signal remained nulled even after the 3D coronary imaging acquisition. Therefore, we hypothesize that the proposed sequence optimized for Gd-BOPTA may also enable tissue characterization with the same patient preparation as with EC-GBCAs and a single contrast bolus, with no need for dedicated or cumbersome mixed double contrast protocols (e.g. EC-GBCAs for perfusion/delayed enhancement followed by an intravascular agent for vascular imaging), a known limitation of “blood-pool” contrast agents (BP-CAs) imaging (10). Importantly, no heavy venous enhancement was seen with sequence B, which has been described to complicate interpretation of coronary imaging with BP-CAs (30).

Coronary imaging in children is especially challenging due to their smaller size, small contrast bolus, relatively higher cardiac output and the potential for image degradation due to limited patient cooperation during the critical time window for image acquisition with EC-GBCAs. The advent of high-relaxivity agents with prolonged intravascular transit can improve blood-background tissue differentiation thus facilitating visualization of the smaller coronary arteries, including the more distal branches. Gd-BOPTA has been shown to improve diagnostic coronary CMRA in adults, and its efficacy and safety profile makes it an appealing choice for coronary imaging in pediatric patients. Moreover, the use of Gd-BOPTA and the described sequence design is an attractive alternative to streamline CMR studies by enabling in a single examination detailed functional (ischemia/viability) and anatomical (coronary) assessment. The incremental diagnostic value of combined CA imaging, myocardial perfusion and late gadolinium enhancement using a versatile agent such as Gd-BOPTA has already been shown in adults (10).

Limitations

A number of limitations need to be acknowledged. First, although powered to identify any statistical significant difference between the two sequences, this was a single-center study performed in a center of expertise. Also, all scans were performed under general

anesthesia following the institutional practice and in the setting of a multidisciplinary clinical planning. This access to specialized personnel and equipment resources is not widely available and local practices vary. Nevertheless, general anesthesia ensured prolonged cooperation, reliable breathing pattern as well as less HR fluctuations. If on the one hand this might affect the transferability of the results to non-anesthetized pediatric studies, on the other hand this allowed an objective head-to-head comparison of two similarly defined sequences, whilst assessing for potential confounding factors such as HR changes/gating efficiency during the two different acquisitions (no differences in HR and acquisitions lengths were noted). We have previously demonstrated that the gating approach used improves coronary imaging in awake adult patients with CHD (18). We hypothesize that such improvement is likely to occur in awake pediatric scans but this remains to be proven. Notably, this protocol could also be adapted to other MRI vendors and help to streamline the imaging service delivery.

In this study we have not assessed the diagnostic accuracy of the proposed sequence to screen for coronary stenosis/anomalies. On one hand, this was not a predefined study endpoint. On the other hand, there were not enough coronary anomalies in this study population to report on the accuracy of each sequence to be able to detect them. This would require a larger sample and, ideally, validation with invasive data, which without clinical justification was deemed unethical in a cohort of pediatric patients. However, we expect that the increase in spatial resolution attained with this high-relaxivity contrast agent and sequence design would help to reduce flow-induced signal voids, partial volume artifacts or velocity-shear effects. This would allow a more accurate diagnosis and estimation of the severity of a coronary stenosis, particularly in the proximal segments, as demonstrated previously (31,32).

Finally, we have not tested the proposed protocol at higher field strength, which also has been shown to result in higher spatial resolution, SNR and CNR values between blood

and myocardium. However unreliable ECG-triggering due to amplified magneto-hydrodynamic effects, frequent susceptibility artifacts, and increased T1 radiofrequency field distortions are known drawbacks.

ACCEPTED MANUSCRIPT

CONCLUSIONS

The use of Gd-BOPTA with an IR 3D-SSFP sequence design that benefits of its attributes of high-relaxivity and prolonged intravascular time results in improved coronary imaging visualization in small infants and young children with high HR and within a clinically acceptable scan time. This approach may allow replacing invasive cardiac catheterization for diagnostic coronary imaging and preoperative planning in pediatrics thus reducing the risks associated with such procedures.

DECLARATIONS:

Ethics approval and consent to participate:

The study was approved by the local institutional research ethics committee (South East London Research Ethic Committee, 10/H0802/65). Written informed consent was obtained from all participants' parents/guardians prior to scanning.

Consent for publication:

Written informed consent was obtained from the legal parent or guardian to publish any anonymised individual patient data related to this research.

Competing interests:

This study was supported in part by Bracco Imaging. However, Bracco Imaging had no control on the recruitment stage, the inclusion or analysis of data and information that might present a conflict of interest.

Funding:

The authors acknowledge support from a British Heart Foundation (BHF) programme grant (RG/12/1/29262), the European Research Council under the European Union's Seventh Framework Programme (FP/2007-2013) / ERC Grant Agreement n. 307532, BHF New Horizons program (NH/11/5/29058), and the United Kingdom Department of Health via the National Institute for Health Research (NIHR) comprehensive Biomedical Research Centre award to Guy's & St Thomas' NHS Foundation Trust in partnership with King's College London and King's College Hospital NHS Foundation Trust.

Author's contributions:

GG, RB were involved in the conception and design of the study. MSV, MH, TH, GG participated in the collection of data. MH was the leading physicist that conducted all the initial phantom work that ultimately enabled the development and improvement of the MRI sequence used in this manuscript. MSV, MH, ND, VSV TH, RB, GG were involved in the analysis and interpretation of data. MSV was responsible for the drafting of the manuscript. MSV, MH, ND, VSV, AB, SM, KP, CAF, TH, RB, GG were involved in the revision of the manuscript. All authors read and approved the final manuscript and agreed with the dual authorship.

REFERENCES

1. Tangcharoen T, Bell A, Hegde S et al. Detection of coronary artery anomalies in infants and young children with congenital heart disease by using MR imaging. *Radiology* 2011;259:240-7.
2. Valsangiacomo Buechel ER, Grosse-Wortmann L, Fratz S et al. Indications for cardiovascular magnetic resonance in children with congenital and acquired heart disease: an expert consensus paper of the Imaging Working Group of the AEPC and the Cardiovascular Magnetic Resonance Section of the EACVI. *Eur Heart J Cardiovasc Imaging* 2015;16:281-97.
3. Bunce NH, Lorenz CH, Keegan J et al. Coronary artery anomalies: assessment with free-breathing three-dimensional coronary MR angiography. *Radiology* 2003;227:201-8.
4. Wang Y, Rossman PJ, Grimm RC, Riederer SJ, Ehman RL. Navigator-echo-based real-time respiratory gating and triggering for reduction of respiration effects in three-dimensional coronary MR angiography. *Radiology* 1996;198:55-60.
5. Henningsson M, Smink J, Razavi R, Botnar RM. Prospective respiratory motion correction for coronary MR angiography using a 2D image navigator. *Magn Reson Med* 2013;69:486-94.
6. Piccini D, Monney P, Sierro C et al. Respiratory self-navigated postcontrast whole-heart coronary MR angiography: initial experience in patients. *Radiology* 2014;270:378-86.
7. Wu HH, Gurney PT, Hu BS, Nishimura DG, McConnell MV. Free-breathing multiphase whole-heart coronary MR angiography using image-based navigators and three-dimensional cones imaging. *Magn Reson Med* 2013;69:1083-93.

8. Taylor AM, Dymarkowski S, Hamaekers P et al. MR coronary angiography and late-enhancement myocardial MR in children who underwent arterial switch surgery for transposition of great arteries. *Radiology* 2005;234:542-7.
9. Bi X, Carr JC, Li D. Whole-heart coronary magnetic resonance angiography at 3 Tesla in 5 minutes with slow infusion of Gd-BOPTA, a high-relaxivity clinical contrast agent. *Magn Reson Med* 2007;58:1-7.
10. Klein C, Gebker R, Kokocinski T et al. Combined magnetic resonance coronary artery imaging, myocardial perfusion and late gadolinium enhancement in patients with suspected coronary artery disease. *J Cardiovasc Magn Reson* 2008;10:45.
11. Hu P, Chan J, Ngo LH et al. Contrast-enhanced whole-heart coronary MRI with bolus infusion of gadobenate dimeglumine at 1.5 T. *Magn Reson Med* 2011;65:392-8.
12. Makowski MR, Wiethoff AJ, Uribe S et al. Congenital heart disease: cardiovascular MR imaging by using an intravascular blood pool contrast agent. *Radiology* 2011;260:680-8.
13. Stuber M, Botnar RM, Danias PG et al. Contrast agent-enhanced, free-breathing, three-dimensional coronary magnetic resonance angiography. *J Magn Reson Imaging* 1999;10:790-9.
14. Saeed M, Wendland MF, Higgins CB. Blood pool MR contrast agents for cardiovascular imaging. *J Magn Reson Imaging* 2000;12:890-8.
15. Yun H, Jin H, Yang S, Huang D, Chen ZW, Zeng MS. Coronary artery angiography and myocardial viability imaging: a 3.0-T contrast-enhanced magnetic resonance coronary artery angiography with Gd-BOPTA. *Int J Cardiovasc Imaging* 2014;30:99-108.

16. Sakuma H, Ichikawa Y, Suzawa N et al. Assessment of coronary arteries with total study time of less than 30 minutes by using whole-heart coronary MR angiography. *Radiology* 2005;237:316-21.
17. Cavagna FM, Maggioni F, Castelli PM et al. Gadolinium chelates with weak binding to serum proteins. A new class of high-efficiency, general purpose contrast agents for magnetic resonance imaging. *Invest Radiol* 1997;32:780-96.
18. Henningsson M, Hussain T, Vieira MS et al. Coronary MR angiography using image-based respiratory motion compensation with inline correction and fixed gating efficiency. *Mag Reson Med* 2017. (published online ahead of print 20 March). Available at doi: 10.1002/mm.26678. (Accessed 25th August 2017).
19. Yu J, Agarwal H, Stuber M, Schar M. Practical signal-to-noise ratio quantification for sensitivity encoding: application to coronary MR angiography. *Journal of magnetic resonance imaging. J Magn Reson Imaging* 2011;33:1330-40.
20. Etienne A, Botnar RM, Van Muiswinkel AM, Boesiger P, Manning WJ, Stuber M. "Soap-Bubble" visualization and quantitative analysis of 3D coronary magnetic resonance angiograms. *Magn Reson Med* 2002;48:658-66.
21. Botnar RM, Stuber M, Danias PG, Kissinger KV, Manning WJ. Improved coronary artery definition with T2-weighted, free-breathing, three-dimensional coronary MRA. *Circulation*. 1999 Jun 22;99(24):3139-48.
22. Leipsic J, Abbara S, Achenbach S et al. SCCT guidelines for the interpretation and reporting of coronary CT angiography: a report of the Society of Cardiovascular Computed Tomography Guidelines Committee. *J Cardiovasc Comput Tomogr* 2014;8:342-58.

23. Uribe S, Hussain T, Valverde I et al. Congenital heart disease in children: coronary MR angiography during systole and diastole with dual cardiac phase whole-heart imaging. *Radiology* 2011;260:232-40.
24. Bland JM, Altman DG. Statistical methods for assessing agreement between two methods of clinical measurement. *Lancet* 1986;1:307-10.
25. Landis JR, Koch GG. The measurement of observer agreement for categorical data. *Biometrics* 1977;33:159-74.
26. Henningsson M, Koken P, Stehning C, Razavi R, Prieto C, Botnar RM. Whole-heart coronary MR angiography with 2D self-navigated image reconstruction. *Magn Reson Med* 2012;67:437-45.
27. Shen Y, Goerner FL, Snyder C et al. T1 relaxivities of gadolinium-based magnetic resonance contrast agents in human whole blood at 1.5, 3, and 7 T. *Invest Radiol* 2015;50:330-8.
28. Hazirolan T, Gupta SN, Mohamed MA, Bluemke DA. Reproducibility of black-blood coronary vessel wall MR imaging. *J Cardiovasc Magn Reson* 2005;7:409-13.
29. Ni Y. in *Clinical Cardiac MRI*. 2nd Edition. Germany: Springer Heidelberg; 2012. pp. 31–51. ISBN 978-3-642-23034-9.
30. Stillman AE, Wilke N, Li D, Haacke M, McLachlan S. Ultrasmall superparamagnetic iron oxide to enhance MRA of the renal and coronary arteries: studies in human patients. *J Comput Assist Tomogr* 1996;20:51-5.
31. Schneider G, Ballarati C, Grazioli L et al. Gadobenate dimeglumine-enhanced MR angiography: Diagnostic performance of four doses for detection and grading of carotid, renal, and aorto-iliac stenoses compared to digital subtraction angiography. *J Magn Reson Imaging* 2007;26:1020-32.

32. Yang Q, Li K, Liu X et al. Contrast-enhanced whole-heart coronary magnetic resonance angiography at 3.0-T: a comparative study with X-ray angiography in a single center. *J Am Coll Cardiol* 2009;54:69-76.

FIGURES LEGENDS

Figure 1. CMRA reformatted images from six randomly selected patients with their demographic details, average HR, acquisition duration and image quality parameters depicting areas of improved visualization. Left-hand panels - sequence A (pre-contrast). Right-hand panels - sequence B (post-contrast). Arrows point to coronary segments with improved visualization after contrast. DORV, double outlet right ventricle; CoA, aortic coarctation; PAPVR, partial anomalous venous return; TGA, transposition of the great arteries; ToF, tetralogy of Fallot; VSD, ventricular septal defect.

Figure 2. VWS and qualitative score results for both the pre-contrast (A) and post-contrast sequences (B).

Figure 3. Coronary arteries qualitative score distribution for sequence A and B.

Figure 4. VWS and qualitative score results for both the pre-contrast (A) and post-contrast sequences (B), for of each coronary artery.

Figure 5. Scatter plots showing no correlation between VWS and potential image detrimental factors such as age, BSA and HR.

TABLES

Table 1. Image quality grading system	
1 - Poor-quality 2 - Marked blurring	Non-diagnostic
3 - Moderate blurring 4 - Minimal blurring 5 - Sharply defined borders	Diagnostic

Table 2. Patient characteristics		
Age (years)	6 ± 2.8 [2;12]	
Gender	29 male (73%); 11 female (27%)	
BSA (Kg/m²)	0.75 ± 0.31	
Clinical Indication	Aortic coarctation/interrupted arch	7
	Tetralogy of Fallot/Pulmonary atresia	6
	ASD/VSD	3
	HLHS	3
	Pulmonary atresia	3
	TGA	2
	PAPVR	2
	Ebstein's anomaly	1
	Common arterial trunk	1
	Coronary fistula	1
Marfan's syndrome	1	
Complex CHD	10	
		N=40

Table 3. CMRA parameters	Sequence A (pre)	Sequence B (post)	p value	95% Confidence Interval of the Difference
Acquisition duration (minutes)	5.3 ± 1.8	5.2 ± 1.5	0.532	[-0.218, 0.415]
Heart rate (bpm)	78 ± 14.7 [56-109]	78 ± 14.5 [54-114]	0.443	[-0.644, 1.444]
Mean vessel length (cm)	5.2 ± 1.8	6.4 ± 2.0	<0.001	[- 1.670, - 0.772]
Average vessel diameter (mm)	2.2 ± 0.2	2.2 ± 0.2	0.922	[- 0.055, 0.061]
Signal to noise ratio	12.6 ± 4.4	31.1 ± 7.4	<0.001	[-188.478, -128.625]
Contrast to noise ratio	9.0 ± 1.8	13.5 ± 3.7	<0.001	[- 7.244, -4.306]
Coronary arteries vessel sharpness	0.53 ± 0.07	0.56 ± 0.07	0.001	[- 0.045, - 0.012]

Table 4. Coronary arteries anomalies identified

Main clinical diagnosis	Coronary anomaly
Single outlet right ventricle	Single coronary
Transposition of the great arteries	Anomalous origin of the RCA from the LAD
Tetralogy of Fallot	Dual LAD supply
Tricuspid stenosis	Single coronary
Coronary-cameral fistula	RCA fistula to left atrium

Table 5. Coronary arteries average qualitative score and non-diagnostic segments

Coronaries	Segments	Sequence A		Sequence B		p value	
		Score	Non-diagnostic	Score	Non-diagnostic	Score	Non-diagnostic
All Coronaries	All Segments	3.8 ± 0.59	42 (13.1%)	4.1 ± 0.53	33 (10.3%)	<0.001	0.002
LAD	All	3.9 ± 0.98	9 (7.5%)	4.2 ± 0.96	8 (6.7%)	0.009	0.566
	Proximal	4.5 ± 0.72	0	4.8 ± 0.45	0	0.002	>0.999
	Mid	4.2 ± 0.83	2	4.2 ± 0.79	1	0.670	0.323
	Distal	3.2 ± 0.91	7	3.6 ± 1.08	7	0.01	>0.999
LCx	All LCx	3.6 ± 1.11	20 (25%)	4.0 ± 1.11	14 (17.5%)	0.005	0.019
	Proximal	4.2 ± 0.87	3	4.7 ± 0.48	0	0.002	0.083
	Mid and distal	3.3 ± 1.10	17	3.7 ± 1.19	14	0.002	0.002
RCA	All RCA	3.9 ± 1.03	13 (10.8%)	4.1 ± 1.09	11 (9.2%)	0.037	0.033
	Proximal	4.5 ± 0.60	0	4.7 ± 0.55	0	0.088	0.323
	Mid	3.6 ± 1.02	3	3.8 ± 1.14	3	0.042	0.160
	Distal	3.2 ± 1.06	10	3.4 ± 1.15	8	0.192	0.183

SUPPLEMENTARY MATERIAL

Figure 1. Soap-Bubble user interface. A reformatted CMRA image is generated (viewport 4) after manually tracking in three orthogonal views (viewports 1 to 3) the coronary artery path (yellow crosses). The vessel length is measured along the validated user-specified points in the reformatted coronary artery as described by Etienne A et al (2002) (20).

Figure 2. Examples of consensual image quality scores given by the two independent readers to each coronary segments of the LAD (panel A), LCx (panel B) and RCA (panel C).

Figure 3. Bland-Altman plots showing the intra-observer agreement for the qualitative coronary assessment of sequence A and B. The mean bias and 95% limits of agreement (± 1.96 SD) are presented.

Figure 4. Bland-Altman plots depicting the inter-observer agreement for the coronary scoring system used for qualitative assessment of both sequence A and B. The mean difference and 95% limits of agreement (± 1.96 SD) are presented.

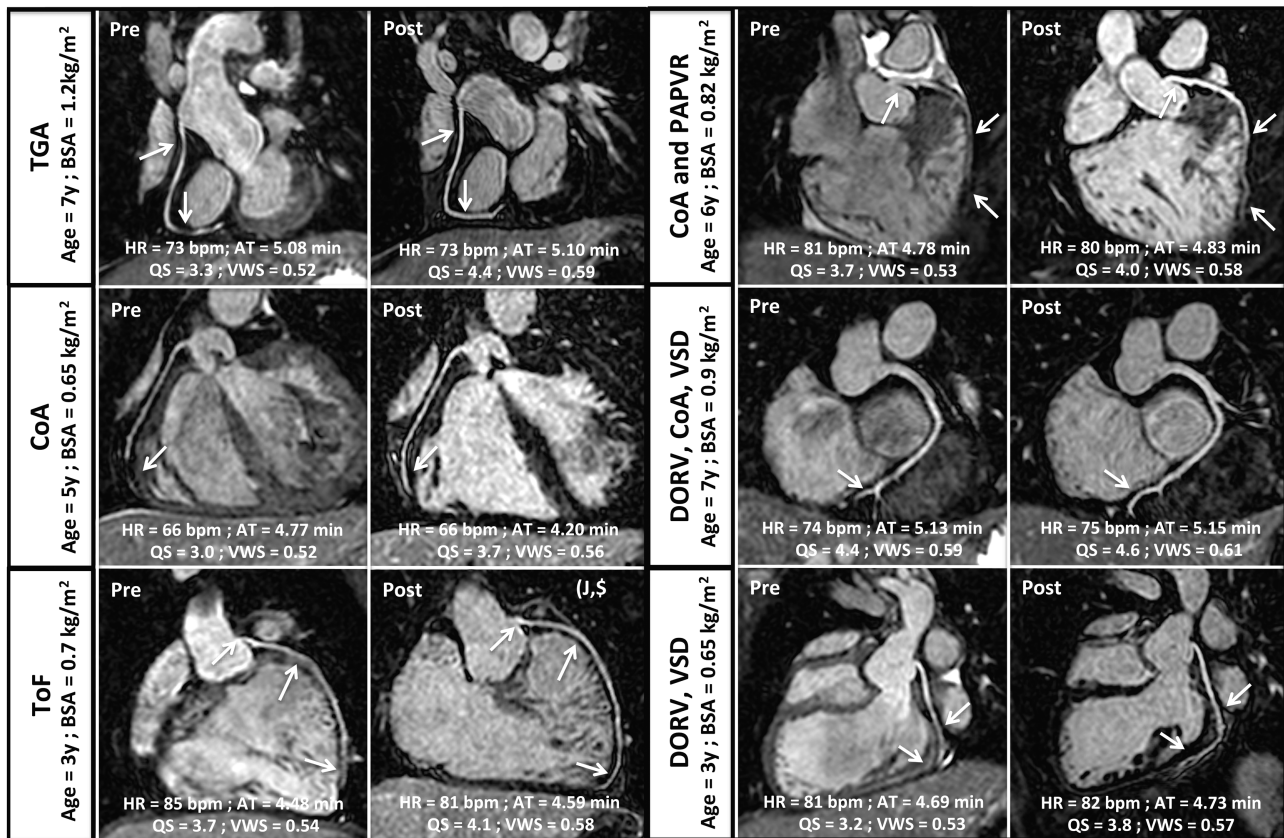


Figure 1

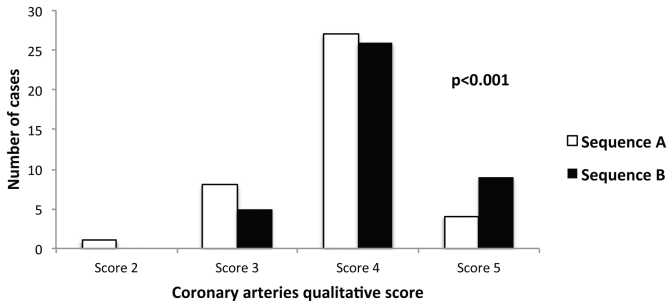
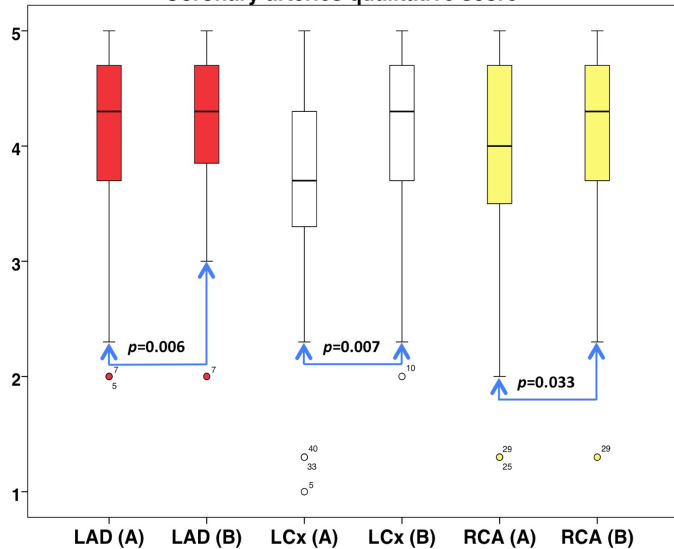


Figure 2

Coronary arteries qualitative score



Vessel wall sharpness by coronary segment

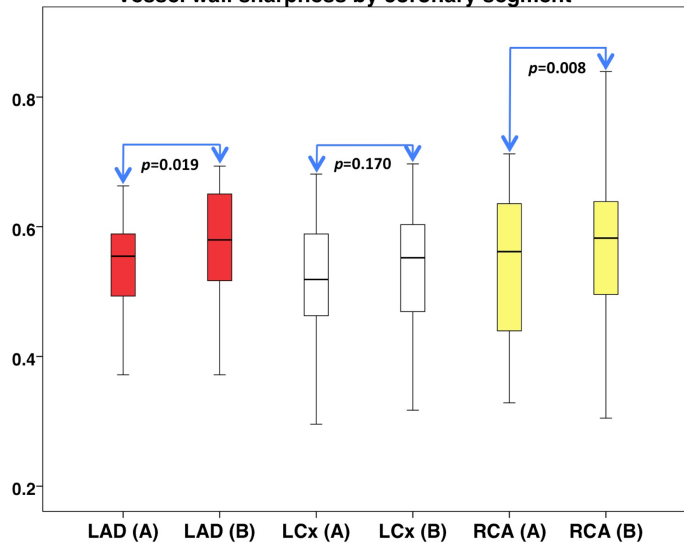


Figure 3

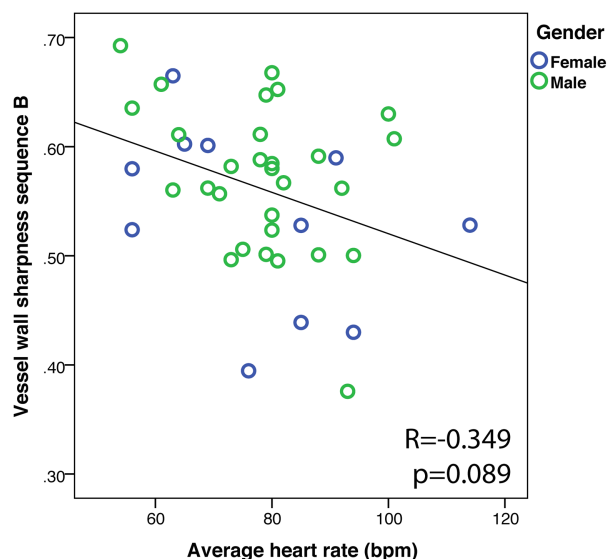
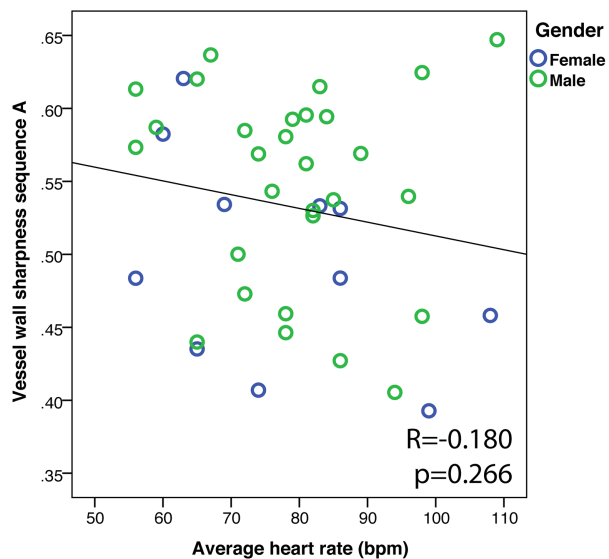
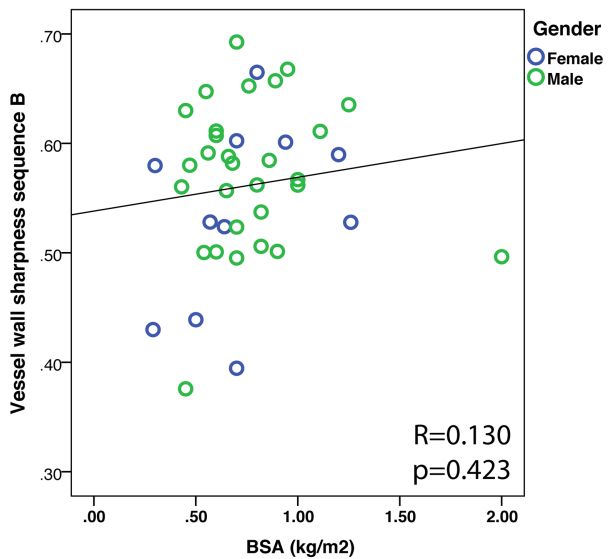
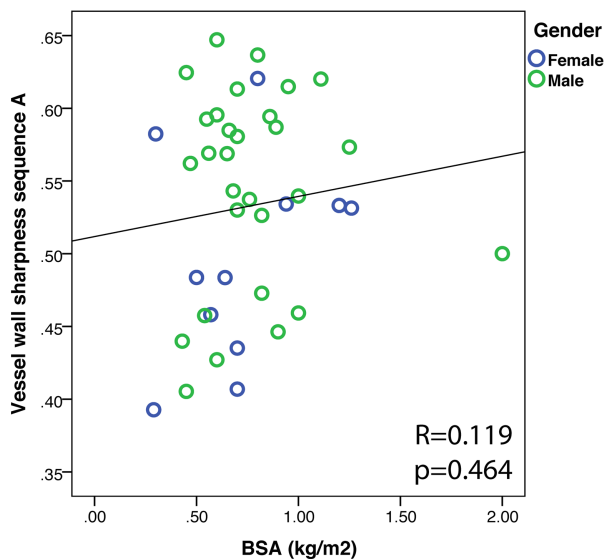
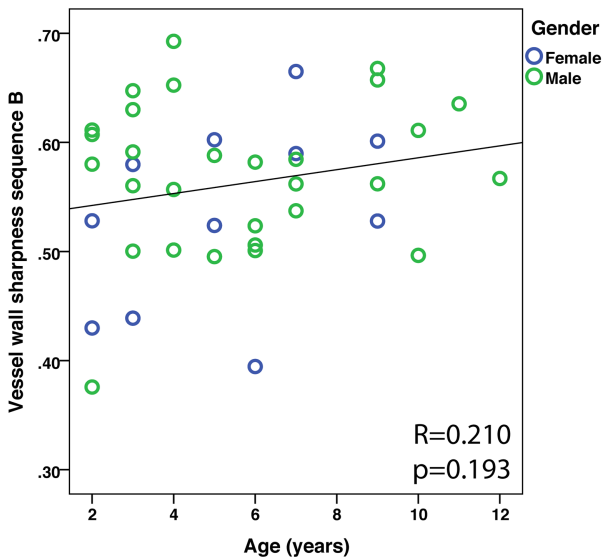
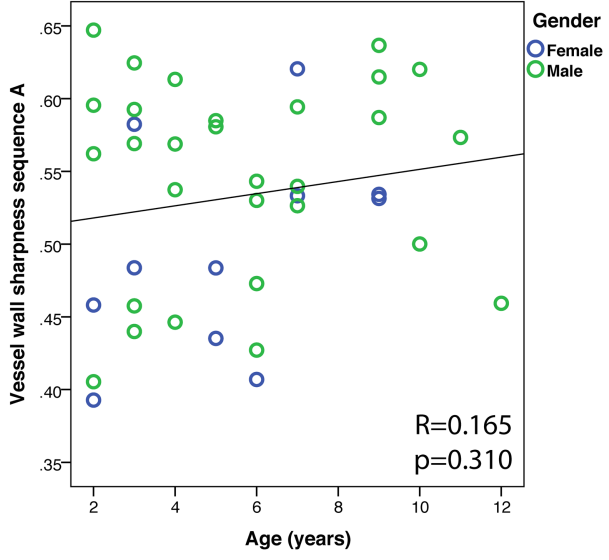
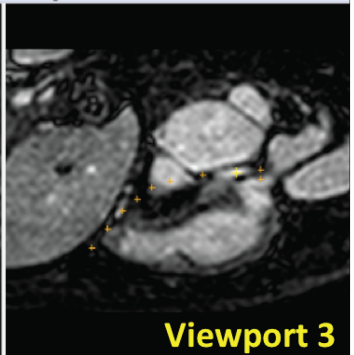
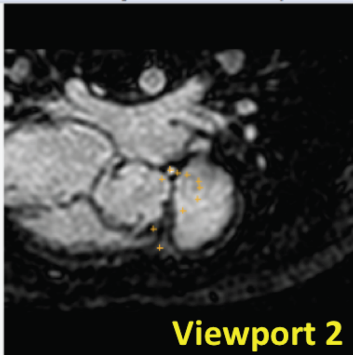


Figure 4



Move Up Move Down Zoom In Zoom Out Move Out Move In Center Move Left Move Right Black Blood

Accept Tracked Points

Track Dist: 0 - +

Undo Point(s)

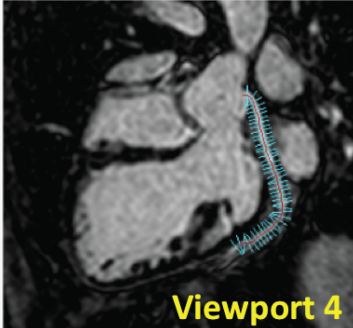
Clear Points

Window 1000

Level 0

TVSCL Contrast

Lines



Automatic Update Reformat

Zoom In Zoom Out Update

Projection Maximum Intensity

Skin Thickness: 0.700 - +

Skin Offset: 0 - +

Smooth Triangulation

Mode: Vessel Tracking

Length [mm]: 74.196064

New Length Measurement

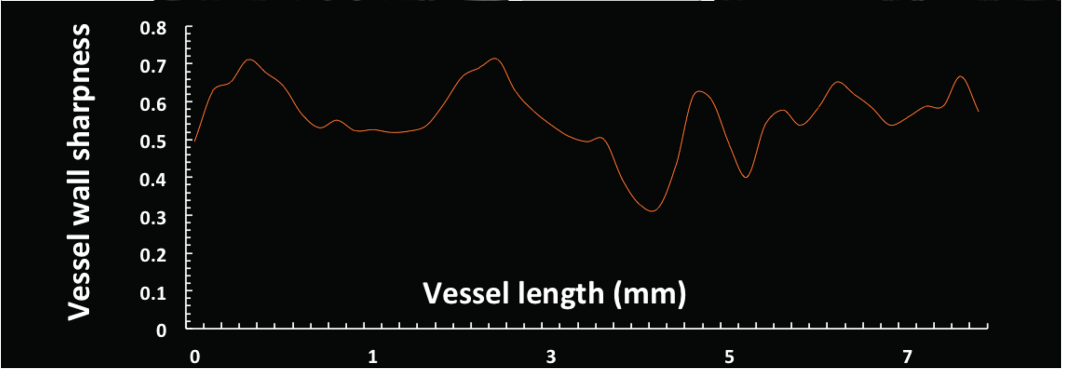
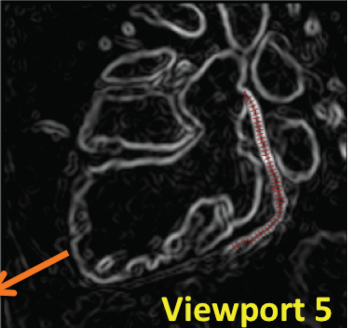


Figure 5

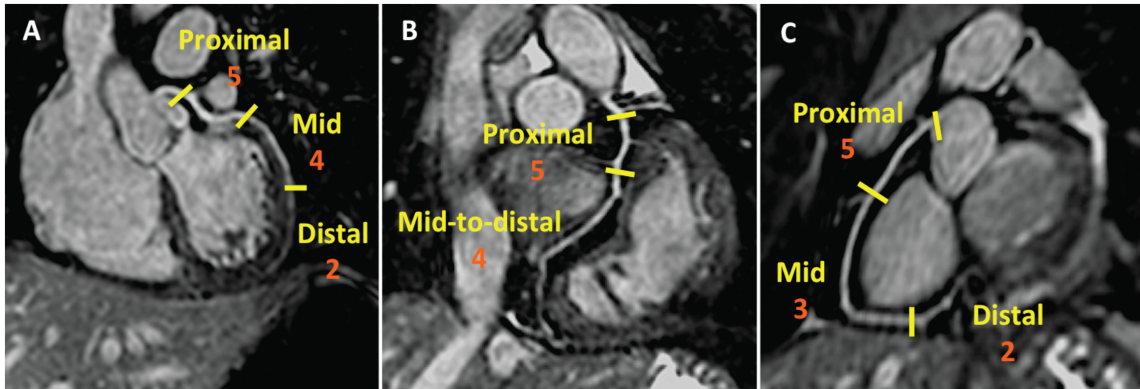


Figure 6

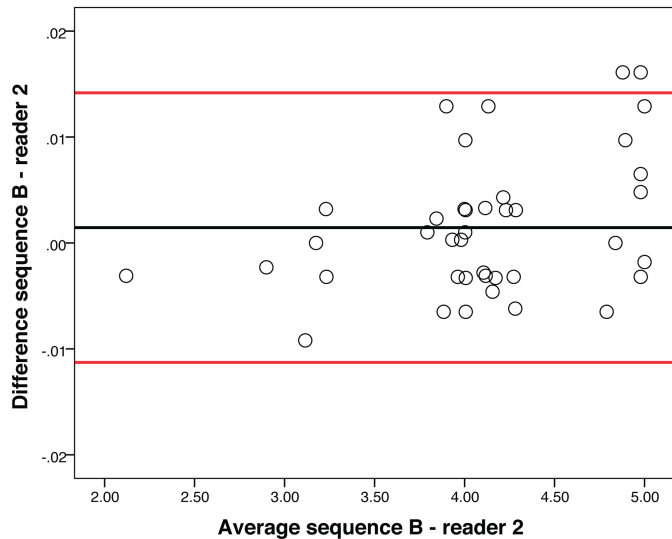
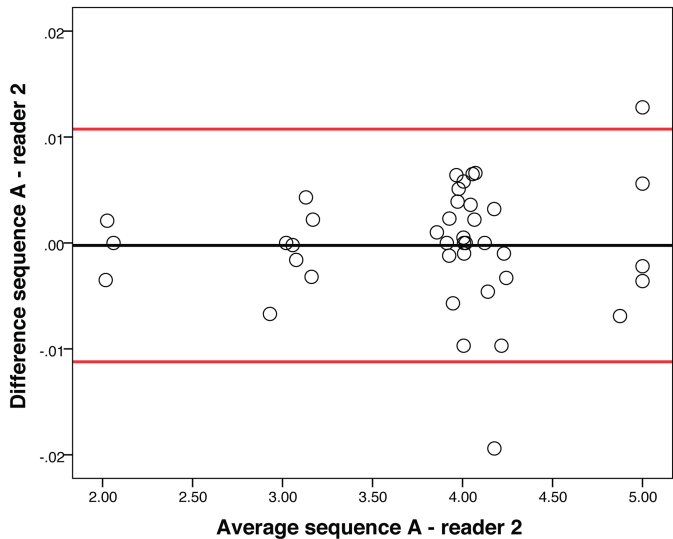
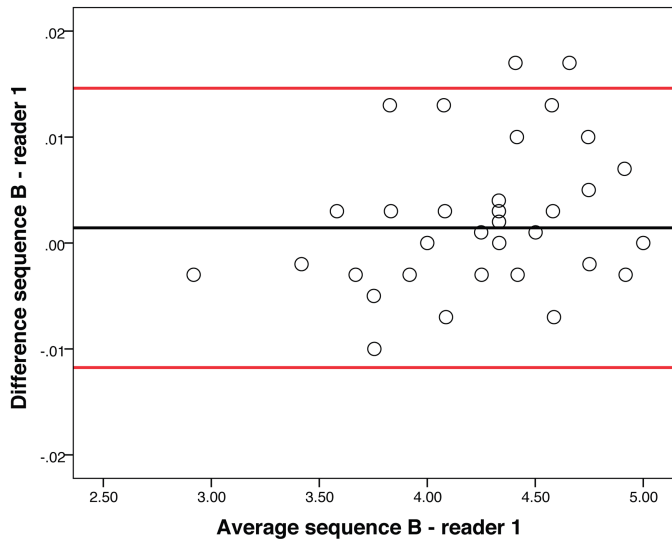
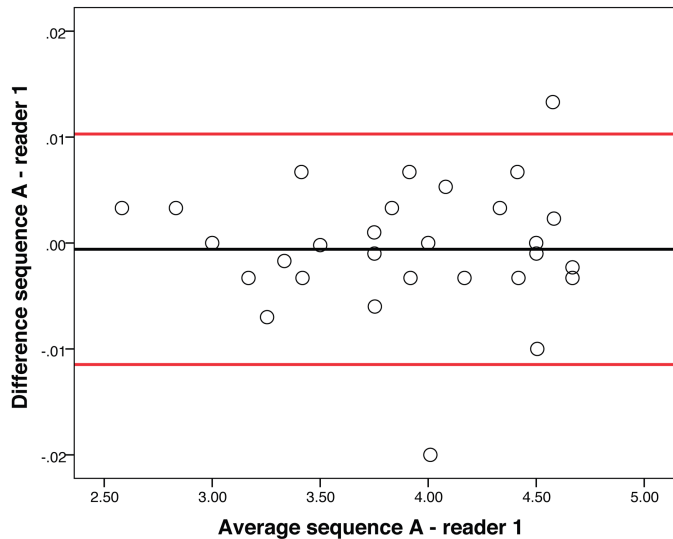


Figure 7

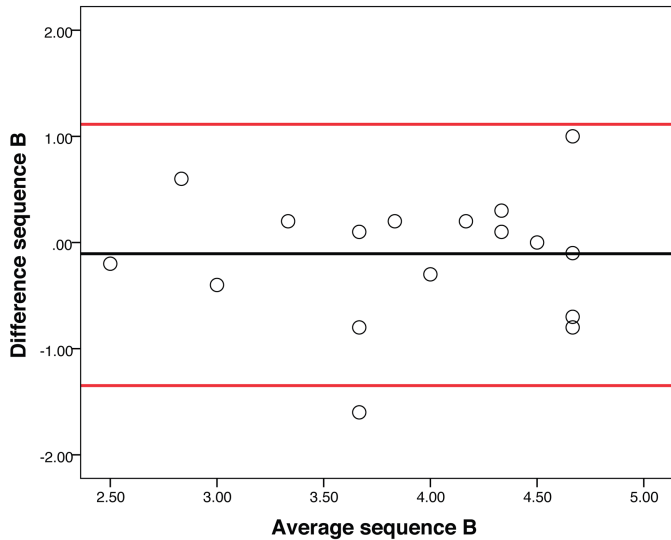
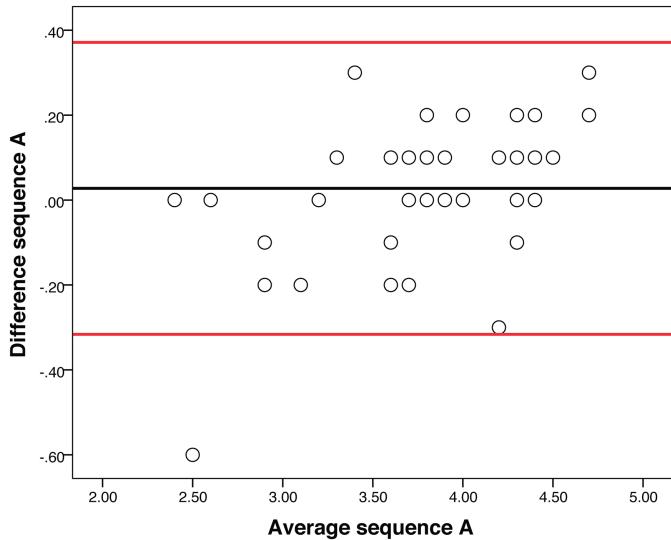


Figure 8